Effects of Polarity of Polymers on Conformation and Lubricating Film Formation of Adsorbed Films

*Yuxi Song[a], *Kenji Fukuzawa[a], Tomoko Hirayama[b], Naoki Yamashita[b], Norifumi L. Yamada[c], Shintaro Itoh[a], Naoki Azuma[a], Hedong Zhang[d]

[a] Department of Micro-Nano Mechanical Science and Engineering, Nagoya University, Furo-cho, Chikusa-ku, Nagoya, 464-8603, Japan

[b] Department of Mechanical Engineering and Science, Kyoto University, Katsura, Nishikyo-ku, Kyoto 615-8540, Japan

[c] Neutron Science Division, High Energy Accelerator Research Organization (KEK), 203-1 Shirakata, Tokai, Naka, Ibaraki 319-1106, Japan

[d] Department of Complex Systems Science, Nagoya University, Furo-cho, Chikusa-ku, Nagoya, 464-8601, Japan.

KEYWORDS

Polymer adsorption; Polarity; Ellipsometry; Neutron reflectivity; Film thickness; Lubrication

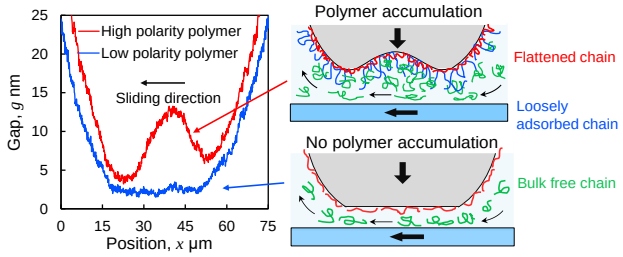

for Table of Contents use only

ABSTRACT

The conformations and lubricating film formation ability of adsorbed films on metal surfaces formed by polyalkylmethacrylate (PAMA) homopolymers with different polarities from non-polar lubricant oil were investigated. It was found that as the polarity of the polymers became higher, the chains in the adsorbed films adsorbed more loosely to the surfaces (i.e., they formed more loops and tails). The loosely adsorbed chains temporarily trapped free polymer chains flowing into the gap between sliding surfaces, resulting in a much thicker lubricating film. Thus, the sliding surfaces were better protected from wear caused by direct contact. On the other hand, flattened chains occupying in the adsorbed film formed by low polarity-polymers could not trap free polymer chains, resulting in a thinner lubricating film.

INTRODUCTION

Adsorbed films of polymers on solid surfaces are of great interest not only for their peculiar properties different from the bulk state, but also for their applications, e.g., cellulose nanocrystals[1], biotissues[2], and drug delivery[3]. In the lubrication field, polymer additives have been used as friction modifiers to improve lubrication performance and reduce wear under severe working conditions. Under the severe conditions (e.g., low speeds, high loads), a thick lubricating film between solid surfaces is always desired during sliding to prevent wear caused by direct contact between solid surfaces. It has been found that a thicker lubricating film were generated when certain polymer additives are added to the lubricant oil, a phenomenon which was suggested to be due to adsorption of polymers on solid surfaces. Without the need for any further thermal annealing treatment, the spontaneously formed adsorbed films are able to prevent direct contact between sliding solid surfaces and thereby reduce wear and friction[4,5].

Among the numerous polymers, polymethacrylates (PMAs) have attracted attention for their beneficial effects not only as viscosity modifiers (VMs), but also in reducing wear by forming adsorption films. The initial studies on PMAs suggested that only the functionalized block copolymer type has the ability to form thick lubricating film during sliding[6,7]. This conclusion is reasonable since the functionalized end of the chains adsorbs to the surface, while the unfunctionalized parts stretch into lubricant oils, resulting in thick brush-like or mushroom-like films on the surfaces[8]. On the other hand, random copolymers and homopolymers had been believed to only form thin pancake-like films that cannot protect surfaces.

However, recent studies have found that, with high enough polarity, even adsorbed films formed by random copolymers and homopolymers via physisorption can present a thick lubricating

boundary film to protect surfaces from wear during sliding[9–11]. Indeed, random copolymers and homopolymers with high polarity are able to form adsorbed films with a double-layer conformation from dilute solutions via physisorption[12–16]; the loosely adsorbed chains can be desorbed from surface by rinsing with solvent, while the flattened chains irreversibly adsorb to the solid surfaces. However, the thickness of the flattened layer is only several nanometers even after longtime annealing[17–20]. How could such a thin layer be able to protect metal surfaces with roughnesses of tens of nanometers or more? Even more surprisingly, the films adsorbed via physisorption are highly durable; they can survive shearing with several hundred megapascals of pressure[9,21]. Currently, only a qualitative understanding of this phenomenon has been achieved: the higher durability of the adsorbed films is caused by the stronger bonding between polymers with higher polarity and metal surfaces. The difficulty lies in in-situ characterization of the adsorbed films from the lubricant oil, especially their thickness, which is a key parameter in determining their conformation and ability to separate solid surfaces.

Ellipsometry is widely used to measure the thicknesses of adsorbed films of polymer melts[17,22–24]. However, the similar refractive indexes of the polymer and lubricant oil (mainly alkane) make it difficult to measure thickness in-situ by ellipsometry. Recently, through the measurement of gaps between solids filled with the adsorbed polymer film, we developed a method for in-situ measurement of the thickness of adsorbed film under pressure that uses the vertical-objective-based ellipsometric microscopy (VEM)[25], which can measure of the temporal changes in thickness during adsorption with a time resolution of 10 s.

In this study, we used VEM and neutron reflectometry to investigate the effect of the polarity of polyalkylmethacrylate (PAMA) polymer on the conformation of film adsorbed via physisorption

and attempted to uncover the reason why polymer with higher polarity can generate a thicker lubricant film during sliding.

EXPERIMENTAL SECTION

Polymer Solutions. Three kinds of PAMA polymer additives with different polarities (poly (stearyl methacrylate) (PMA-C18, Mw = 18 kg/mol, Mw/Mn = 1.30)), poly (lauryl methacrylate) (PMA-C12, Mw = 18 kg/mol, Mw/Mn = 1.41), and poly (2-ethylhexyl methacrylate) (PMA-C8 (EH), Mw = 18 kg/mol, Mw/Mn = 1.38) were used, as shown in Scheme 1. The difference between the polymers is the alkyl chain length, and the number of carbon atoms in the alkyl group of each polymer is indicated in the abbreviation. The longer the alkyl length, the lower the polarity of the polymer. Thus, PMA-C8 (EH) has the highest polarity, followed by PMA-C12 and PMA-C18. The polymers were dissolved into Group III mineral lubricant oil (mainly alkanes) with a concentration of 2.0 wt%. The polymers and lubricant oil were provided by ENEOS Corporation, Japan. The properties of the polymer solutions are listed in Table 1.

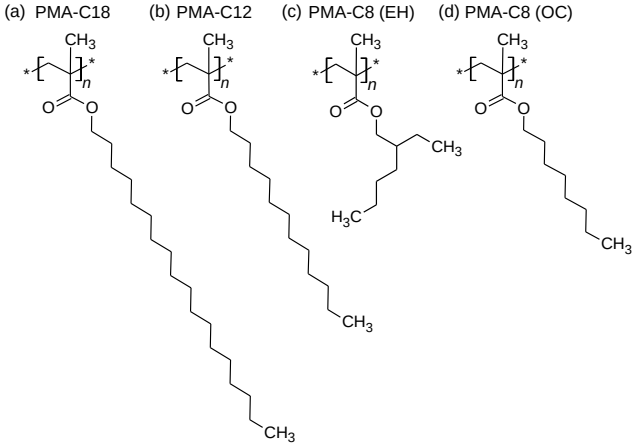

Scheme 1. Chemical Structure of (a) Poly (stearyl methacrylate) (PMA-C18), (b) Poly (lauryl methacrylate) (PMA-C12), (c) Poly (2-ethylhexyl methacrylate) (PMA-C8 (EH)), and (d) Poly (n-octyl methacrylate) (PMA-C8 (OC))

Table 1. Physical Properties of PAMA Polymer Solutions

Solution	PMA-C18	PMA-C12	PMA-C8 (EH)
Density, g/cm3 (15℃)	0.835	0.836	0.836
Kinematic viscosity, mm2/s (40℃)	20.6	20.2	20.4
Viscosity Index	135	137	137

VEM. In the conventional ellipsometry setup, the incident light cannot be reflected at the interface between the lubricant oil and adsorbed polymer film due to the similar refractive indices of the polymer and the lubricant oil. As a result, the polarization state of the reflected light would not change with the thickness of the adsorbed polymer film. Therefore, the thickness of the adsorbed film cannot be measured in-situ with the conventional ellipsometry setup. In order to apply the ellipsometry measurement, the adsorbed polymer films must be isolated from the lubricant oil. In this study, we isolated the adsorbed film in lubricant oil using VEM. The thickness of the adsorbed films under pressure and gap during sliding can be obtained by VEM. The schematic setup of VEM is shown in Scheme 2 (a). The details of the VEM setup can be found in the Supporting Information (Section S2). The ellipsometry optical system was placed under the glass substrate, and the incident light was reflected at the gap between the metal-coated slider and glass substrate. Meanwhile, the objective lens was set perpendicular to the sample surface. This allows real-time observation of the nanometric gap with the high lateral resolution (0.1 μm order) and a wide field of view (100 μm in diameter)[26–29]. Glass (K-LaSFn23 glass, Sumita Optical Glass, Japan) with a refractive index of 1.93 and a thickness of 0.8 mm is used as the substrate. The slider is a plano-convex glass lens (SLB-05-30P, Sigmakoki, Japan) coated

with 53 nm-thick stainless steel (SUS) by sputtering. Its radius is 15.6 mm. The surface roughness (R_a) of the slider and the glass substrate are 0.8 nm and 0.3 nm, respectively.

In this study, the polymer films that adsorbed on the surfaces were isolated from the lubricant oil by squeezing the lubricant oil out of the gap between the surfaces. The procedures for measuring the thickness of the adsorbed film under pressure are as follows (Scheme 2 (a)): The slider was separated from the glass substrate, allowing the polymer additives to adsorb onto the solid surfaces. After maintaining the separation for a certain period of time (~ 10 s), the slider was firmly pressed onto the glass substrate. The gap between the slider and glass substrate was then measured by VEM while the slider was under pressure. When the slider was pressed, only the adsorbed film remained in the contact area because the lubricant oil was squeezed out of the contact area between the slider and the glass substrate during the pressing process. Therefore, the measured gap of the contact area at that moment was equal to the thickness of the adsorbed film. By repeating this procedure of separating and pressing, the temporal change in the thickness of the adsorbed film during adsorption can be obtained. The load applied during the measurement was 25.5 mN. In the measurement, a circular area with a diameter of 10 μm was averaged at the contact center and used to observe the film thickness change. This was done to reduce the error and improve the resolution caused by surface roughness. The resolution and measurement accuracy were about 0.3 nm[25]. More details of the procedures for adsorbed film thickness measurement under pressure are described in our previous work[25].

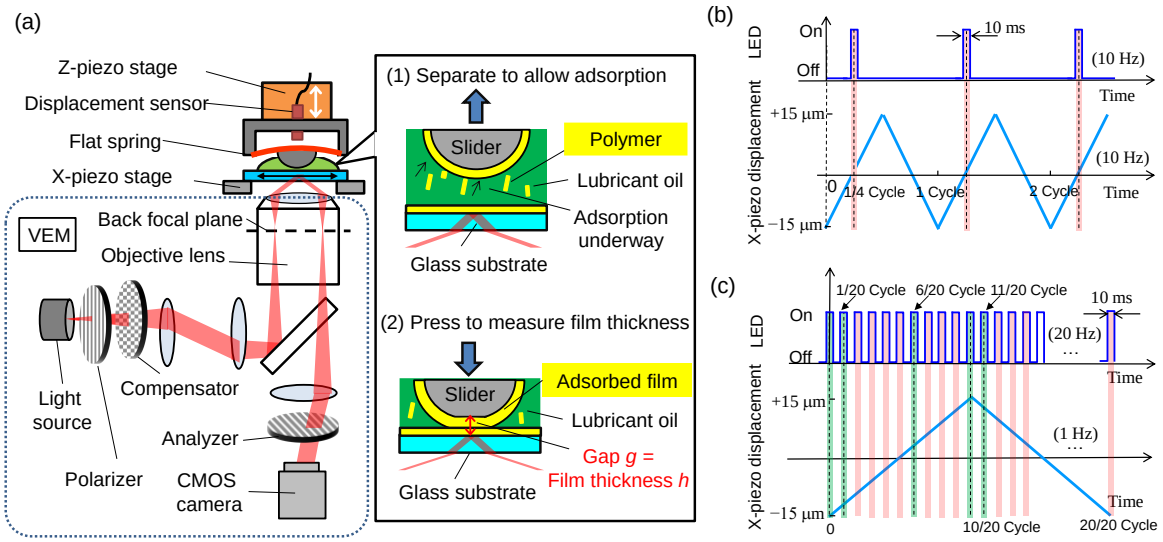

Scheme 2. (a) Schematic Setup for Measuring Adsorbed Film Thickness and Gap During Sliding. (b) Stroboscopic Imaging Setup of Measuring Gap at Sliding Frequency of 10 Hz (Image Capture: 1 frame/sliding cycle). (c) Stroboscopic Imaging Setup of Measuring Gap at Sliding Frequency of 1 Hz (Image Capture: 20 frames/sliding cycle)

In addition to the adsorbed film thickness measurement, the sliding gap between the glass substrate and the slider during sliding under different loads was measured by stroboscopic imaging (Scheme 2 (b), and (c)). The glass substrate was slid reciprocally on an x-piezo stage (P-733.2DD, Physik Instrumente, Germany) with an amplitude of 15 μm. The sliding speed could be changed by varying the frequency of the stage. The loads and mean pressures of the contact area during each sliding movement were 2.55 mN (11.9 MPa), 7.65 mN (17.2 MPa), 12.75 mN (20.4 MPa), 17.85 mN (22.7 MPa), and 25.5 mN (25.6 MPa), respectively. The changes in the gap with the sliding cycle were measured. All the experiments were conducted at room temperature (20 ℃ ~ 25 ℃).

Neutron Reflectometry (NR). With the NR measurement, not only the thickness, but also the density profile of the adsorbed film in the lubricant oil can be obtained in situ, from which the

information on the conformation of the adsorbed films can be obtained. In addition, VEM measurement requires external pressured to be applied on the adsorbed film, while NR measurement can be performed under atmospheric pressure. Therefore, by comparing the thickness by VEM under pressure and the thickness by NR without pressure, the load-bearing ability of the adsorbed films can be obtained.

The NR measurement was conducted using the soft interface analyzer (SOFIA) horizontal-type neutron reflectometer at the Materials and Life Science Experimental Facility of J-PARC[30]. The schematic setup and scattering length density (SLD) values used in the fitting analysis are shown in Scheme 3[21,31,32]. In these measurements, the solvent was replaced with non-polar deuterated hexadecane (D-hexadecane) (Cambridge Isotope Laboratories, USA) to improve the contrast between the polymer and the lubricant oil. PMA-C18 (Mw = 18 kg/mol, Mw/Mn = 1.3), PMA-C12 (Mw = 18 kg/mol, Mw/Mn = 1.40), and poly (n-octyl methacrylate) (PMA-C8 (OC), Mw = 18 kg/mol, Mw/Mn = 1.38) were purchased from Polymer Source, Inc. Although the structure of PMA-C8 (OC) (Scheme 1(d)) used in the NR experiments is slightly different from that of the PMA-C8 (EH) (Scheme 1(c)) used in the VEM experiments, the number of carbon atoms in the alkyl group of these two polymers is the same, indicating that these two polymers have similar polarity. In addition, more than 90% of the composition of the Group III oil used in VEM measurement is nonpolar alkanes. This suggests that the solubilities of PAMAs in hexadecane and Group III oil are similar. The substrate was 30-nm-thick Fe film (R_a: 0.5nm)sputtered on a mirror polished silicon block (50 × 50 × 10 mm, R_a: 0.2 nm) by the ion beam sputtering system at Kyoto University Reactor (KUR-IBS)[33]. After sputtering, the blocks were stored in a vacuum chamber to prevent oxidation. The incident angles θ of the measurement were 0.3, 0.6, and 1.2°. The measurements were carried out 15 min after the solutions were injected into the sample

holder. These measurements obtained the profiles of reflectivity against the scattering vector Q_Z. Q_Z was calculated as $Q_z = 4\pi\sin(\theta/\lambda)$, where θ is the incident angle and λ is the wavelength of the incident neutrons. The obtained NR reflectivity profiles were then analyzed and fitted using GenX 3.6[34]. The experiments were conducted at 25 °C. More details on the fitting of NR measurement are described in the Supporting Information (Section S3).

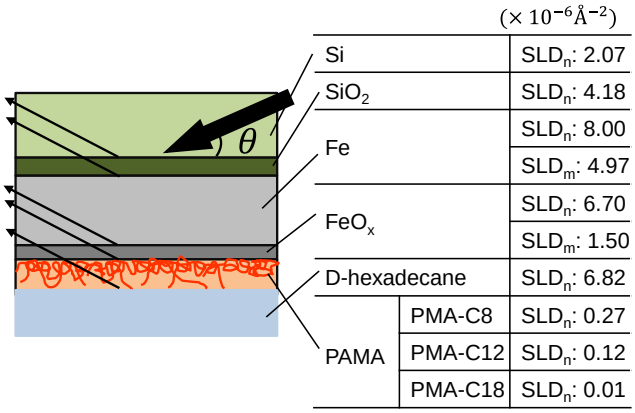

Scheme 3. Schematic Setup of Neutron Reflectometry Measurement

Hansen Solubility Parameters (HSPs) Measurement. To evaluate the polarities of the polymers and the solubilities in hexadecane, the HSPs measurements were performed[35]. As will be discussed in the Results and Discussion section, the strong correlation between solubilities and conformations of adsorbed polymer films was found. In the HSPs theory, the total cohesive energy, E, of a material (the energy required to break all intermolecular forces) can be divided into three separate parts:

$$E = E_D + E_P + E_H \quad (1)$$

where E_D is the dispersive component, E_P is the polar component, and E_H is the hydrogen bonding component[36]. The square of the total solubility parameter or the cohesive energy density δ^2 ($\delta^2 = \frac{E}{V}$) then can be obtained by dividing by the molar volume V:

$$\frac{E}{V} = \frac{E_D}{V} + \frac{E_P}{V} + \frac{E_H}{V} \quad (2)$$

$$\delta^2 = \delta_D^2 + \delta_P^2 + \delta_H^2 \quad (3)$$

whereδ_D, δ_P, and δ_H are the experimentally measurable HSPs corresponding to dispersive interactions, polar interactions, and hydrogen bonding interactions, respectively. The solubility of a polymer in the solvent can then be evaluated by the HSP distance R_a between the polymer and the solvent:

$$R_a = \sqrt{4\left(\delta_{D,polymer} - \delta_{D,solvent}\right)^2 + \left(\delta_{P,polymer} - \delta_{P,solvent}\right)^2 + \left(\delta_{H,polymer} - \delta_{H,solvent}\right)^2} \quad (4)$$

The smaller R_a, the more likely the polymer and solvent are thermodynamically compatible in the solution. To determine if a polymer could be dissolved in a particular solvent, one can define a sphere with the center coordinates (δ_D, δ_P, δ_H) and radius R_0 in a three-dimensional coordinate system. The coordinates of a good solvent should lie within this sphere, i.e., the relative energy difference (RED):

$$RED = \frac{R_a}{R_0} \quad (5)$$

should be less than 1 for a good solvent. The smaller the RED distance from the solvent, the more likely the polymer can be dissolved in it.

In this study, the HSPs and R_0 of PMA-C18, PMA-C12, and PMA-C8 (OC) were measured using the Hansen Solubility Parameter in Practice (HSPiP) software. For each polymer, the solubility was analyzed at room temperature (20 °C ~ 25 °C) in 37 solvents with known HSPs. The measured HSPs, R_0, for each polymer and the RED distance from hexadecane (δ_D: 16.3, δ_P: 0, δ_H: 0) are listed in Table 2. Among these polymers, the δ_D did not change much. This suggests that the intermolecular dispersion forces are similar since these polymers have similar molecular weights. On the other hand, the shorter the length of the alkyl group of the polymer, the higher the δ_P was found, indicating the higher dipolar intermolecular forces (polarity). The δ_H also increased slightly when the alkyl group of the polymer was shorter. The 37 solvents used in this study (Table S1) and the details for the measurement are described in the Supporting Information (Section S1).

Table 2. HSPs for PAMAs and RED Distance from Hexadecane

Sample	δ_D ($MPa^{0.5}$)	δ_P ($MPa^{0.5}$)	δ_H ($MPa^{0.5}$)	R_0 ($MPa^{0.5}$)	RED
PMA-C18	18.0	2.7	1.4	7.7	0.59
PMA-C12	17.9	3.6	1.9	7.2	0.72
PMA-C8 (OC)	17.5	5.0	2.8	6.7	0.93

RESULTS AND DISCUSSION

Adsorbed Film Thickness and Conformation. The results of the neutron reflectivity measurements for PMA-C8 (OC), PMA-C12, and PMA-C18 solutions are shown in Fig. 1 (a), where the solid lines are optimal fitting results and the open symbols are experimental results.

The SLD depth profiles for each of the adsorbed films were obtained from the fitting results, as shown in Fig. 1 (b), where the horizontal axis is the distance from the Fe surface. Assuming incompressibility and additivity of PAMA polymers and D-hexadecane mixture, the volume fraction of PAMA polymer ϕ in each layer of the films was calculated as $\mathrm{SLD} = \mathrm{SLD}_{\mathrm{PAMA}} \times \phi + \mathrm{SLD}_{\mathrm{D-hexadecane}} \times (1 - \phi)$. Extremely small SLD values at the Fe surface were found in all cases, indicating that all three polymer chains were adsorbed on the surface. The differences lied in the upper layers of the films. The SLD of the upper layer in the case of PMA-C18 suddenly increased to the value for a bulk PAMA solution. On the other hand, in the cases of PMA-C12 and PMA-C8 (OC), there existed the upper layers whose SLD values were smaller than that of a bulk solution but larger than those of the pure PAMAs. Therefore, it can be concluded that the adsorbed PMA-C12 and PMA-C8 (OC) films adopted a double-layer conformation, while the PMA-C18 film had a single-layer conformation. The single-layer adsorbed film of PMA-C18 was around 1.2 nm (ϕ: > 99 %) thick. The PMA-C12 film had a 1.8 nm-thick bottom layer (ϕ: > 99 %) and 2.4 nm-thick top layer (ϕ: 12 %). The PMA-C8 (OC) film was much thicker: the bottom layer was around 2.7-nm thick with a ϕ more than 99 %, and the top layer was around 4.5-nm thick with a ϕ of 22 %. The 1.2-nm thickness and over 99% polymer volume fraction indicated that the adsorbed PMA-C18 film had a dense and flattened conformation. Increasing the polarity of the polymer caused the top layer of the adsorbed film to be thicker and have a higher ϕ.

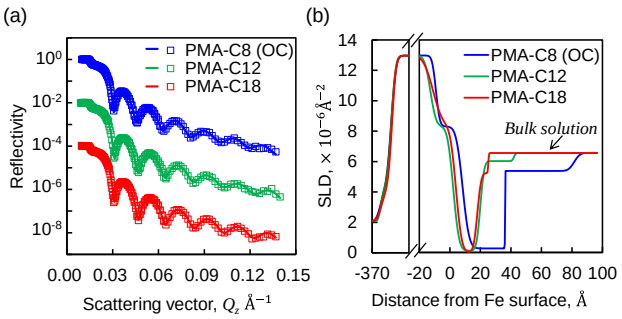

Figure 1. (a) Neutron reflectivity measurements of PMA-C8 (OC), PMA-C12, and PMA-C18 adsorbed films on Fe surface in D-hexadecane. Open symbols show experimental data, and solid lines are fitting results. (b) SLD depth profiles of PMA-C8 (OC), PMA-C12, and PMA-C18 adsorbed films on Fe surface as functions of distance from the Fe surface.

These results suggest that, as the polarity of the polymer increases, the adsorbed film changes from a flat conformation (Scheme 4 (a)) to a double-layer conformation (Scheme 4 (b)). The flattened strongly adsorbed chains occupy the film with the flat conformation, while more loosely adsorbed chains (loops and tails) exist in the film with double-layer conformation. To determine the reason for the difference, the adsorption kinetics of polymers on surfaces will be discussed first, which could be divided into three steps: diffusion to the surface, attachment on the surface, and reconstruction of the conformation[37,38]. In the last step, the polymers spread out on the surface as much as possible to obtain as much energy gain as possible. A previous study suggested that the different spread-out rates in the last step lead to different conformations of the adsorbed films[25]. Thus, the difference in conformations revealed in this study might be interpreted as being due to a difference in the speed at which the polymers “spread out” on surfaces.

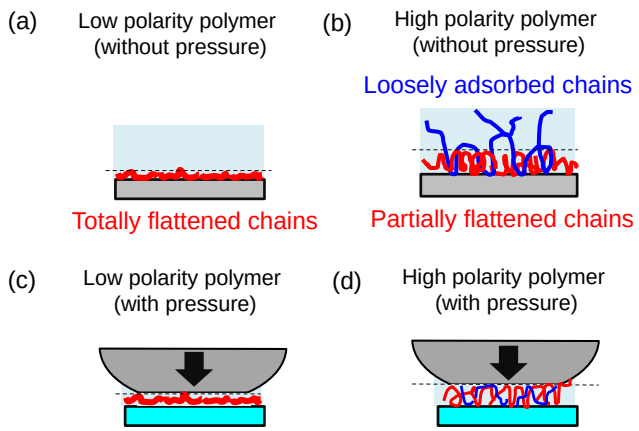

Scheme 4. (a) Schematic Diagram of Polymer with Low Polarity (PMA-C18) Film Adsorbed on Surface Measured by NR (without Pressure). (b) Schematic Diagram of Polymer with High Polarity (PMA-C8) Film Adsorbed on Surface Measured by NR (without Pressure). (c) Schematic Diagram of Polymer with Low Polarity (PMA-C18) Film Adsorbed on Surface Measured by VEM (with Pressure). (b) Schematic Diagram of Polymer with High Polarity (PMA-C8) Film Adsorbed on Surface Measured by VEM (with Pressure).

Both the Group III oil and D-hexadecane solvents used in this study are non-polar, and the higher the polarity of the polymer is, the lower the solubility in these solvents becomes. The solubilities of PAMAs in hexadecane were evaluated by HSPs, as shown in Table 2. The smaller the RED distance from hexadecane, the more likely the polymer can be dissolved in hexadecane. The RED distances of PMA-C18, PMA-C12, and PMA-C8 (OC) from hexadecane were 0.59, 0.72 and 0.93, respectively. Therefore, the lowest solubility of PMA-C8 (OC) polymer causes it to be more like to shrink or curl up on itself in solution, which should result in it taking a longer time to spread out on the surface. Thus, during adsorption, it is more likely for newly arriving PMA-C8 (OC) chains to compete with chains that have already attached themselves to the surface before they were completely flattened. Consequently, not all the chains would have enough room to flatten themselves fully, resulting in more loosely adsorbed chains (loops and tails). This

competition also means that the chains cannot be completely flattened, resulting in a thicker bottom layer measured in NR (the partially flattened chains in Scheme 4 (b)). On the other hand, the PMA-C18 polymers prefer to stretch in solution because of their high solubility, suggesting that they spread out on the surface quickly. Thus, once the chains have become attached to the surface, they quickly flatten out, and the surface quickly becomes covered by dense flattened chains. Even if late-arrival chains are able to adsorb to unoccupied areas left on the surface, they would easily desorb as a result of the limited adsorption sites and the high solubility in the solvent. Therefore, the adsorbed PMA-C18 film is expected to have a flattened conformation. Also, since there is no competition, the chains should be fully flat on the surface, resulting in a thinner layer (the totally flattened chains in Scheme 4 (a)). Note that Zhu et al. found that PMMA (polar) prefers to form a double-layer adsorbed film on sapphire in CCl_4 (non-polar) solvent and a single-layer film in $CHCl_3$ (polar) solvent; the findings reported here could similarly be interpreted as being due to a difference in solubility[39]. The simulation results of Linse also found that a poorer solvent condition causes more tails to form in the adsorbed films[40].

The Flory–Huggins parameters (χ parameters) for different polymers in hexadecane were also calculated with the measured HSPs using[41]:

$$\chi = \alpha \frac{v_{solvent}}{RT}\left(\left(\delta_{D,polymer} - \delta_{D,solvent}\right)^2 + 0.25\left(\delta_{P,polymer} - \delta_{P,solvent}\right)^2 + 0.25\left(\delta_{H,polymer} - \delta_{H,solvent}\right)^2\right) \quad (6)$$

where $v_{solvent}$ is the molar volume of the solvent (cm^3/mol), R is the gas constant (8.314 J/(mol·K)), T is the temperature (in K), and α is a correction factor. Lindvig et al. found that a universal correction factor $\alpha = 0.6$ could be used in the solutions of poly methacrylates (PMAs)[41]. Although the correction factor $\alpha = 0.6$ has not been verified in the solution conditions (2wt% PAMAs/hexadecane) used in this study, the calculation results could still

provide some indication. The calculated χ parameters for PMA-C18, PMA-C12, and PMA-C8 (OC) in hexadecane at room temperature (298.15 K) were 0.37, 0.48, and 0.69, respectively. In General, a solvent was considered as a good solvent when $\chi < 0.5$ and a non-solvent when $\chi > 1$. Figure 2 shows the relationship between χ parameter and the thickness of adsorbed films. The red symbols denote the thickness of the bottom layer of adsorbed films, and the blue symbols denote the total thickness. Compared to the top layers, the volume fractions of polymer chains in the bottom layers were much larger (ϕ: > 99 %). Therefore, the bottom layers contributed most to the adsorption masses. The strong correlation between χ parameter and the bottom layer thickness of the adsorbed films was found. The relationship between the χ parameter and bottom layer thickness can be approximated to a linear function. The bottom layer thickness of also decreased toward 0 as the χ parameter approached 0. This tendency is reasonable: Because when $\chi = 0$, the energy difference between polymer and solvent could be considered as 0. As a result, the polymer/surface and solvent/surface interactions would be the same, and the polymer would not adsorb on the surface.

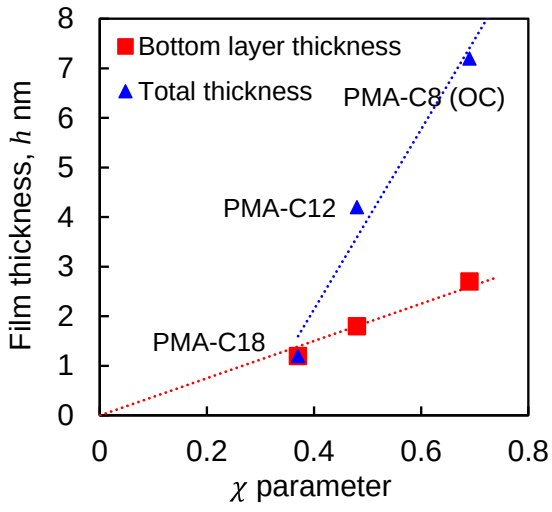

Figure 2. Relationship between χ Parameter and Film Thickness of Adsorbed Films Measured by NR. The Red Symbols Denote the Thickness of the Bottom Layer of Adsorbed Films, and the Blue Symbols Denote the Total Thickness.

We also tried to explain this difference from the perspective of entropy. The polymer chain adsorption can be considered to be the result of competition between the polymer chain's surface-sticking energy gain and translational entropy loss[38]. For the same number of adsorption sites, polymer chains with higher polarity may gain more surface-sticking energy from the higher dipolar forces. The higher energy gain thus compensates for the high translational entropy loss of the polymer chains, suggesting that more polymer chains can be adsorbed. Therefore, since more adsorbed polymer chains can adsorb to the same adsorption sites, a polymer with higher polarity should form more loops and tails.

The temporal changes in the thicknesses of different adsorbed films during adsorption were measured under pressure by VEM, as shown in Fig. 3. The thicknesses of the adsorbed films became stable in less than 100 s. Note that even if the measured thickness became saturated quickly, it may take a much longer time to let the adsorbed films reach equilibrium. The saturation thicknesses of PMA-C18, PMA-C12, and PMA-C8 (EH) were 0.9 nm, 1.5 nm, and 2.8 nm under the load of 25.5 mN. The thicknesses of the adsorbed films under pressure were almost the same as the thicknesses of the corresponding bottom layers on the Fe surface measured by NR (PMA-C18: 1.2nm, PMA-C12: 1.8 nm, and PMA-C8(OC): 2.7 nm) when no pressure was applied to the films. These results suggest that the polymers did not adsorb on the non-polar glass substrate. The reason could be that the gain in energy of the polymer chains from the weak adsorption cannot compensate for their translational entropy loss. The results also indicate that only the dense flattened chains in the bottom layer ($\phi > 99\%$) had a load-bearing ability (Scheme

4 (c), (d)). On the other hand, the volume fractions of polymer chains in the loosely adsorbed layers were very low ($\phi < 25\%$), the polymer chains of the loosely adsorbed layers would collapse when pressure was applied to the films, resulting in thinner thicknesses (Scheme 4(d)).

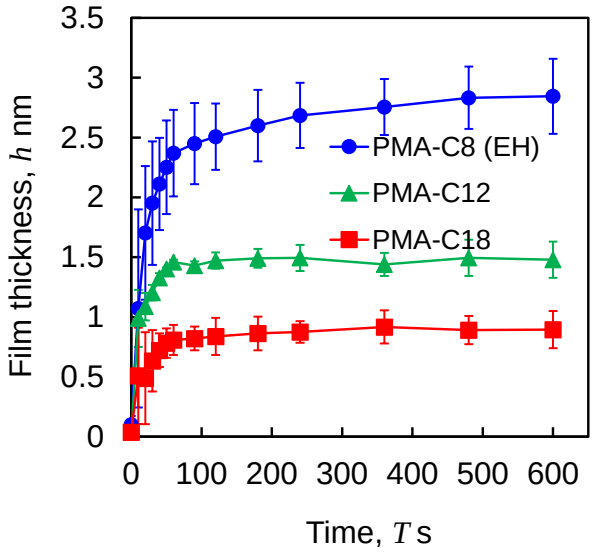

Figure 3. Temporal changes in thickness of PMA-C8 (EH), PMA-C12, and PMA-C18 films adsorbed on SUS surface in Group III oil under a load of 25.5 mN.

Since the top layers of the adsorbed films cannot withstand the load, and the thicknesses of the bottom layers were less than 3 nm, how could such thin films separate the sliding surfaces under pressure? To see how this is possible, the changes in the gap between the slider and glass substrate were measured as the number of sliding cycles was increased.

Lubrication Film Formation Abilities. After the thicknesses of the adsorbed films saturated, the glass substrate was driven by the x-piezo stage in a reciprocating manner at a constant speed of 0.6 mm/s (frequency: 10 Hz). The sliding amplitude was 15 μm. During each sliding cycle, a two-dimensional gap distribution image (one frame) was captured with stroboscopic imaging at the moment of 1/4 cycle (Scheme 2 (b)). The changes in the gap at the center of the contact area

(diameter: ~ 10 μm) versus the number of sliding cycles under different sliding loads are shown in Fig. 4. For PMA-C18 and PMA-C12, the gap between the slider and glass substrate became stable within a few cycles after the sliding started. As the applied load became higher, the gap became smaller; this is a reasonable result because higher loads make it harder for the lubricant oil to flow into the gap. When the sliding load was 25.5 mN, the thickness of generated sliding lubrication film (gap) was almost the same as that of the static adsorbed film under pressure. On the other hand, the case of PMA-C8 (EH) was quite different. When the sliding load was low (2.55 mN), the sliding gap became stable within 20 sliding cycles, whereas under higher sliding loads, the gap increased slowly with the number of sliding cycles. Surprisingly, after several - hundred cycles, the sliding gap under higher loads was larger than that under 2.55 mN. At the end of the sliding, the gap was over 10 nm for all loads. Although the sliding gap stabilized very quickly under 2.55 mN, the 10 nm sliding gap was much larger than those of PMA-C18 and PMA-C8 (EH), which is unusual because the same applied loads and sliding speeds should generate the same hydrodynamic pressure for the liquids with same viscosity. To determine the reason for this difference, gap profiles during sliding were extracted from the captured gap distribution images.

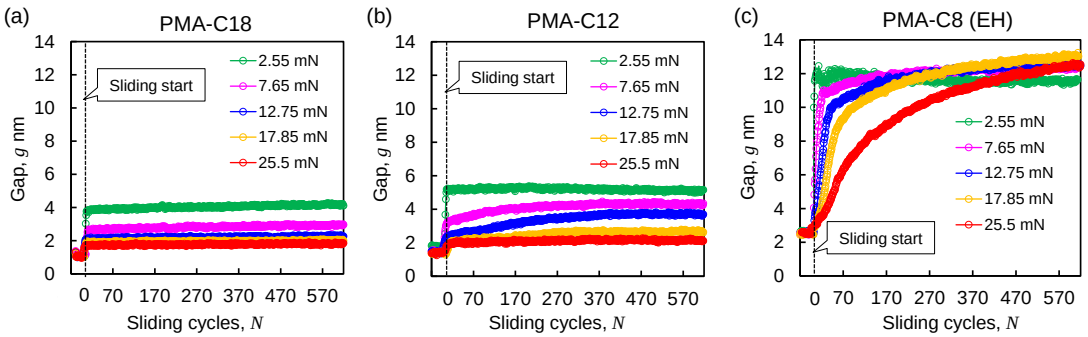

Figure 4. Change in gap at the center of contact area versus number of sliding cycles under loads of 2.55 mN, 7.65 mN, 12.75mN, 17.85mN, and 25.5 mN for (a) PMA-C18, (b) PMA-C12, and (c) PMA-C8 (EH).

The gap distributions along the sliding direction between the slider and glass substrate are shown in Fig. 5 for each PAMA polymer under different sliding loads. The gap profiles were obtained by averaging over a 10-μm-wide area, and the profiles at the 20^{th} (Fig. 5 (a), (c), and (e)), and 600^{th} sliding cycle (Fig. 5 (b), (d), and (f)) are shown. At the 20^{th} cycle, the minimum gap for all PAMAs were decreased as the applied loads increased. In addition, the gap near inlet area of the flow was larger than that around the outlet; this difference was due to nanometric deformations of the slider surface caused by the hydrodynamic pressure of sliding. At the 600^{th} cycle, the gap profiles for PMA-C18 (Fig. 5 (b)) and PMA-C12 (Fig. 5 (d)) were almost the same as those of the 20^{th} cycle (Fig. 5 (a), and (c)). On the other hand, the PMA-C8 (EH) film on the slider surface showed a totally different gap distribution at the 600^{th} cycle: its geometry was concave (Fig. 5 (f)), suggesting deformation of the slider. The gap at the center of the contact area remained almost the same under different loads. In addition, the gap at the center of was even slightly larger under the 25.5 mN load than under 2.55 mN. Note that the slider was hard glass, whose Young's modulus is 79.9 GPa. Moreover, the viscosities of the lubricants were very similar (Table 1), which means that the hydrodynamic pressure should deform the slider surfaces of all of the lubricants in a similar way. Therefore, the unique deformation of the slider surface in the case of PMA-C8 (EH) can only be due to the accumulation of polymers. A similar phenomenon was also reported by Yamada et al.[42].

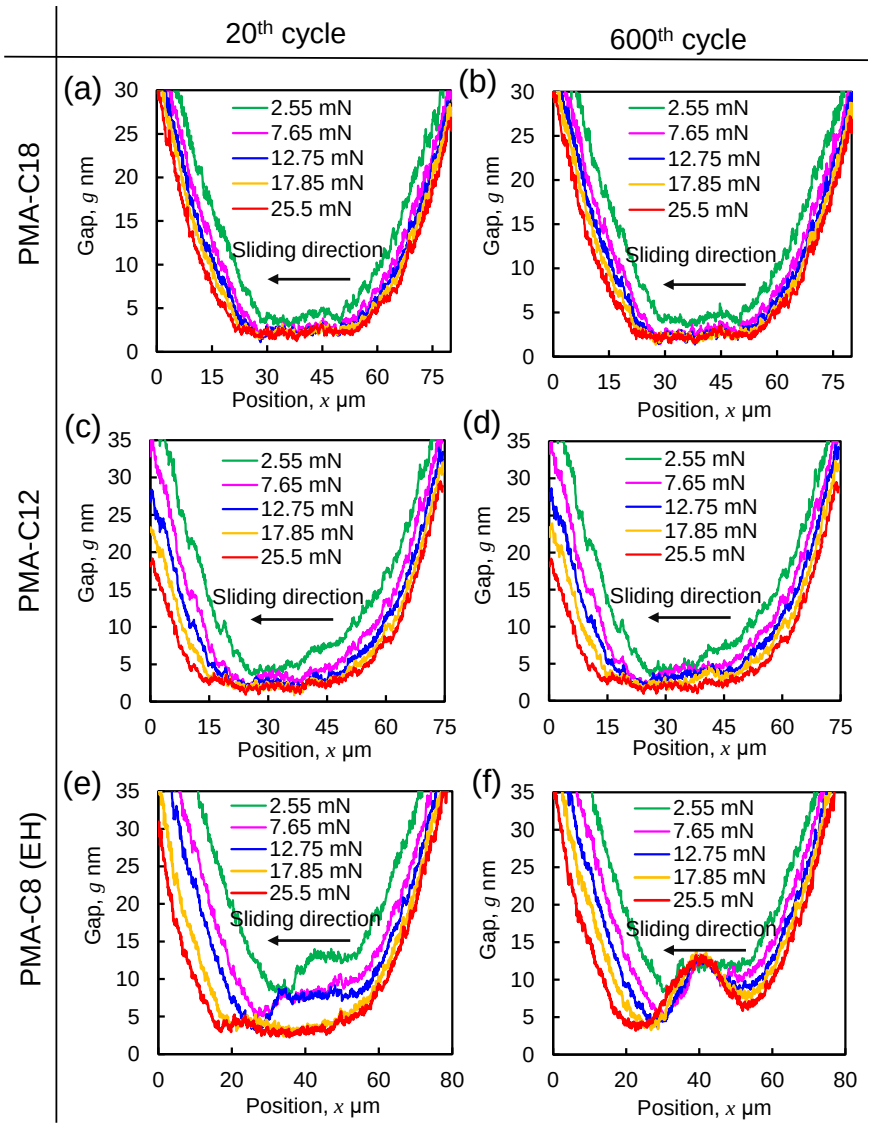

Figure 5. Gap profiles between slider and glass substrate for each PAMA polymer under different sliding loads. (a) PMA-C18 at the 20th sliding cycle, (b) PMA-C18 at the 600th sliding cycle, (c) PMA-C12 at the 20th sliding cycle, (d) PMA-C12 at the 600th sliding cycle, (e) PMA-C8 (EH) at the 20th sliding cycle, and (f) PMA-C8 (EH) at the 600th sliding cycle.

The accumulation in the case of PMA-C8 (EH) could be explained from the conformation of its adsorbed film. In particular, the NR results (Fig. 1) reveal that the adsorbed film had more loosely adsorbed chains. The thickness of the top layer (ϕ: 22 %) was over 4 nm. Recent studies

on interpolymer adhesion of adsorbed films have shown that free bulk polymers can penetrate loosely adsorbed chains. The loosely adsorbed chains act as "connecters" that bridge bulk chains and the substrate, leading to strong adhesion[43–46]. This is in contrast to flattened chains which show "autophobic" behavior with bulk free chains[43], and no adhesion is found between chemically identical polymer chains[44]. Therefore, the loosely adsorbed chains of the PMA-C8 (EH) film could have trapped the free polymer chains that flowed into the gap from outside the contact area, which would have resulted in a larger gap during sliding. Since the motion of the glass substrate was a reciprocating one, the free polymer chains entered from both sides of the contact area. The trapped polymer chains thus accumulated near the center of the gap, resulting in the concave gap distribution.

In this study, the sliding amplitude of the glass substrate was fixed. As the applied load increased, the contact area between the slider and glass substrate also increased, making it harder for free polymer chains to flow into the contact area. Therefore, the gap showed a slower increase with the number of sliding cycles (Fig. 4 (c)). In addition, the larger contact area made it harder to expel polymer chains from the contact area, which can account for why the gap at the center of the contact area under the load of 25.5 mN was slightly larger than that under 2.55 mN (Fig. 5 (f)). In the case of PMA-C18, the adsorbed films had almost no loosely adsorbed chains, and the flattened chains could not trap free chains due to the "autophobic" effect mentioned previously. Therefore, the gap stabilized very quickly after the sliding started (Fig. 4 (a)) and no polymers accumulated (Fig. 5 (a) and (b)).

However, one may suppose that the flattened chains of PMA-C18 film could trap the free polymers and cause accumulation, although no accumulation was found to be due to the desorption of chains from the surface by shearing. The following experiments were conducted in

an attempt to show that the flattened chains of the PMA-C18 film could not have been the cause of the accumulation. The film thicknesses (gap at the center of the contact area) were measured at a load of 25.5 mN just after the sliding motion was stopped at 600 cycles (the open symbols in Fig. 6) and compared with those before sliding (Fig. 3). Figure 6 is divided into two parts: the left side of the double dashed line shows the results of the formation process of the films before sliding (the same as Fig. 3), and the horizontal axis is the time during adsorption process. The right side shows the thickness after each sliding test, and the horizontal axis is the number of sliding tests (each sliding test lasted for 600 cycles). The applied load during each sliding is indicated in the figure. For PMA-C18, it can be seen that the film thicknesses just after sliding were the same as those before sliding. These results suggest that the adsorbed films of PMA-C18 did not desorb even under the highest load (25.5 mN). Therefore, no polymer accumulation occurred in the case of PMA-C18, because the flattened chains could not trap the bulk free chains, not because the flattened chains desorbed from the surface by shearing.

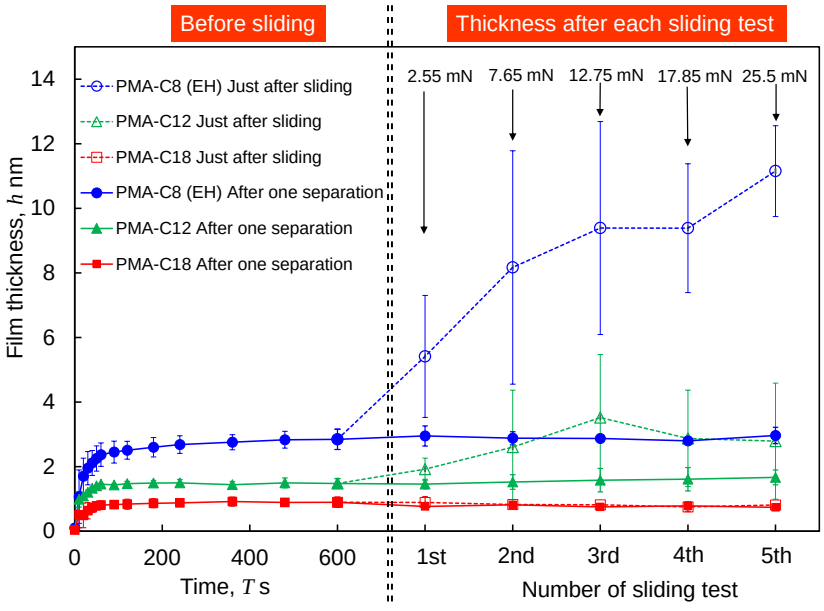

Figure 6. Comparison of film thicknesses of PMA-C8 (EH), PMA-C12, and PMA-C18 before and after sliding. The left side of the double dashed line shows adsorbed film thickness during adsorption. The right side shows film thickness after sliding under loads of 2.55 mN, 7.65 mN, 12.75mN, 17.85 mN, and 25.5mN, where the open symbols are results just after sliding and the filled symbols are the results after one separation.

On the other hand, in the case of PMA-C8 (EH), there was a large increase in the film thickness just after sliding (the blue open symbols in Fig. 6), which was due to polymer accumulation as discussed previously. Since the contact area becomes larger the higher the load, the more difficult it is for the free polymer chains to escape from the contact area. Therefore, as the sliding load increased, the thickness of the film just after sliding also increased. As for the PMA-C12, there was a slight increase in thickness just after sliding (the green open symbols in Fig. 6), suggesting a slight polymer accumulation; this would have been due to it has less loosely adsorbed chains compared with PMA-C8 (EH).

Next, experiments were conducted to see if the trapped polymers remained on the surface. Here, the gap profiles were measured just after sliding. Then, the slider was separated from the glass substrate for a few seconds and then pressed on it again. The gap profiles after this single separation were measured and compared with those just after sliding. Figure 7 shows this comparison for different PAMAs after sliding under the highest load (25.5 mN), where the blue lines are the results just after sliding and the orange lines are those after one separation. For PMA-C18, the gap profiles just after sliding were exactly the same as those after one separation (Fig. 7(a)). For PMA-C12 and PMA-C8 (EH) (Fig. 7 (b), (c)), the gap distribution became ordinary after one separation, indicating that the trapped polymer chains redissolved into the solvent, because such trapped polymer chains caused a large entropy penalty, and it cannot be

maintained in the static condition. The profiles in Fig. 7 (b), (c) also suggested that the accumulated polymers cannot be the already adsorbed polymers. It can be seen that the volume of polymers in the contact area that just after sliding was larger than that after one separation, suggesting that the new (non-adsorbed) polymers were induced in the contact area during sliding. The adsorbed film thicknesses after one separation (gap at the center of the contact area) were compared with those before sliding (compare Fig. 3 with the filled symbols in Fig. 6). The film thickness after sliding was unchanged from that before sliding, which suggests that the conformations of the adsorbed films did not change or quickly returned to the equilibrium state once the pressure was released.

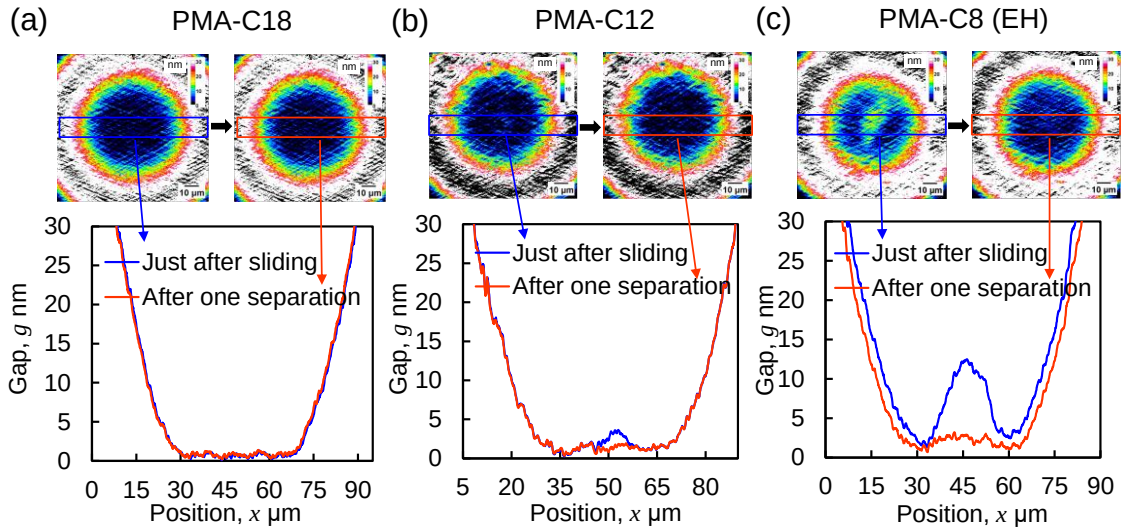

Figure 7. Comparison of gap profiles just after sliding and after one separation for (a) PMA-C18, (b) PMA-C12, and (c) PMA-C8 (EH).

Kinetics of Polymer Accumulation. To observe the details of the PMA-C8 (EH) polymer accumulation process, instead of changing phase of the stroboscopic imaging system (Scheme 2 (b)), 20 frames of gap-distribution images were captured for each sliding cycle (Scheme 2 (c)). The purpose is to prevent error caused by slightly different conditions and drift between different

sliding tests. Due to the limitations of the camera, the sliding frequency was set to 1 Hz (speed: 0.06 mm/s) instead of the 10 Hz in the previous experiments, and the frame rate of the camera then was set to 20 FPS (Scheme 2 (c)). Figure 8 shows the changes in the gap profile during the 200th sliding cycle (sliding frequency: 1 Hz (speed: 0.06 mm/s); sliding load: 12.75 mN). The whole sliding process for the two-dimensional gap distribution and changes in the gap profile can be found in Supplemental movie (Movie S1). At the beginning of sliding, the slider stuck to the glass substrate, so that the position of the contact area moved to the right a little with the speed of the x-piezo stage (Fig. 8(a)). Then, sliding between the slider and glass substrate occurred as the shear strength was achieved, after which the position of the contact area did not change while the glass substrate was still sliding (Fig. 8(b)). During the sliding process, the free polymers outside the contact area flowed into the gap. Because of the interactions with the loosely adsorbed chains of the adsorbed films, the free polymer chains moved at a speed of around 0.03 mm/s, which is more slowly than that of the glass substrate (0.06 mm/s); this movement is reflected in the position changes in the concavity of the contact area in Fig. 8(b). Before these free polymer chains escaped the contact area, the sliding started in the opposite direction (Fig. 8 (c)). Consequently, they became trapped and accumulated at the center of the contact area.

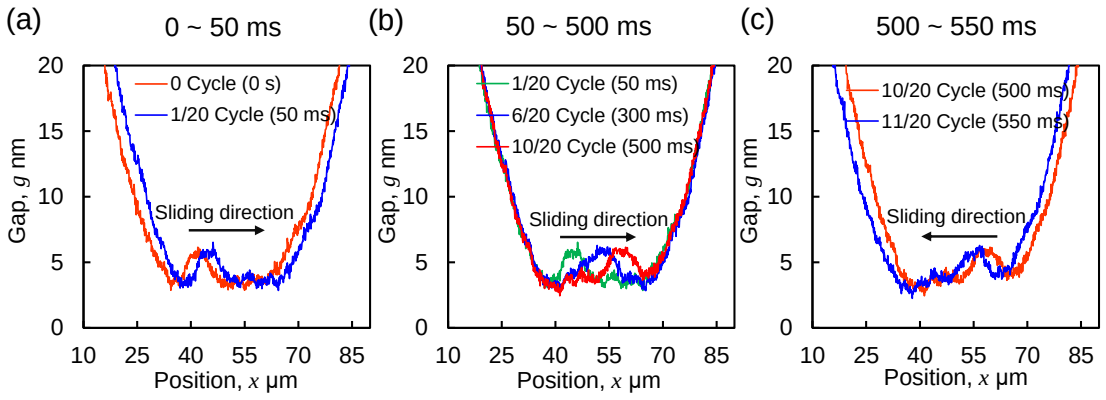

Figure 8. Gap profile changes during the 200th sliding cycle for PMA-C8 (EH) at (a) 0 ~ 50 ms, (b) 50 ~ 500 ms, and (c) 500 ~ 550 ms (applied load: 12.75 mN; sliding speed: 0.06 mm/s (1 Hz)).

On the basis of kinetics, the accumulation of PMA-C8 (EH) polymers should be strongly affected by the sliding speed since they are free polymers. When the sliding speed is low enough, the free polymers should be expelled from the contact area with the movement of the glass substrate. Figure 9 shows the change in the gap versus the number of sliding cycles for different sliding speeds by changing the frequency of the x-piezo stage under a load of 12.75 mN. The green symbols in Fig. 9 are corresponding to the results in Fig. 8. As shown in Fig. 9, the polymer became less likely to accumulate as the sliding speed decreased. In particular, as shown by the red symbols in Fig. 9, when the sliding speed was less than 0.03mm/s (the speed of free polymer chains in the contact area during sliding in Fig. 8), the accumulation phenomenon disappeared.

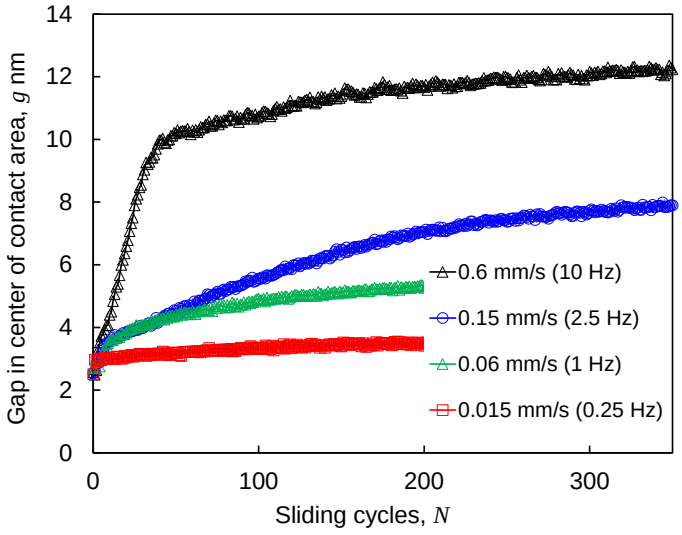

Figure 9. Change in gap versus number of sliding cycles for PMA-C8 (EH) under load of 12.75 mN for sliding speeds of 0.6 mm/s, 0.15 mm/s, 0.06 mm/s, and 0.015 mm/s.

The question of why random copolymer or homopolymer with high polarity can effectively protect surfaces from wear can be answered on the basis of the results presented above. The adsorbed films formed by these polymers have more loosely adsorbed chains (tails and loops). Although these chains cannot withstand much load, they trap free bulk polymers that flow into the gap between the sliding surfaces. As a result, much thicker lubricating films form, which reduces the contact area and prevents direct contact between the surfaces. The trapped polymer chains not only protect the surfaces but also the adsorbed film from being rubbed directly. Thus, friction, especially wear caused by direct contact, can be prevented.

This wear reduction mechanism is different from that of polymer brushes. Polymer brushes grafted on surfaces reduce friction by steric repulsion between molecules[47], and thus the thickness of the lubricating films is limited by the length of the grafted chains. The loosely adsorbed chains can generate thicker lubricating films by trapping free chains especially at higher loads, since the free chains are harder to expel and thus should have better wear reduction performance at high loads.

CONCLUSIONS

We investigated the effect of the polarity of PAMA polymers on the conformation of their films adsorbed from the non-polar solvent on Fe surfaces. Our results showed that an increase in polymer polarity resulted in a higher Flory–Huggins parameter (χ parameter) in hexadecane and a thicker adsorbed film on the surface. The conformation of the adsorbed films also changed from the single layer structure with flattened chains to a double-layer structure with more loosely adsorbed chains (loops and tails). The reason for this transition could be due to the difference in solubility. The solubility of the polymer in the non-polar solvent decreased as its polarity

increased. With lower solubility, the polymer tends to curl up in solution, so it takes a longer time to spread out on the surface during adsorption. As a result, newly arriving polymer chains are more likely to compete with chains that were already attached to the surface before they were completely flattened. Due to this competition, not all the chains would have enough room to flatten themselves fully, resulting in more loosely adsorbed chains (loops and tails).

In terms of the lubricating film formation, the flattened polymer chains of the adsorbed film formed by the low-polarity polymers could not trap the free polymer chains, resulting in thin lubricating film during sliding. In contrast, although the loosely adsorbed polymer chains of the adsorbed films formed by high-polarity polymers could not withstand much load, they trapped bulk free polymer chains that flowed into the gap from outside the contact area during sliding. The trapped free chains could not all be expelled from the gap unless the sliding speed was extremely low. Consequently, much thicker lubricating films formed during sliding. The trapped polymers protected not only the surfaces but also the adsorbed film from direct rubbing, which could answer the question of why adsorbed polymer films with high polarities can reduce wear and have high durability. Our findings thus shed new light on how to design polymer additives in lubricant oils.

ASSOCIATED CONTENT

Supporting Information.

The following file is available free of charge.

Details of Hansen Solubility Parameters Measurement, list of the solvents with known HSPs used in this study, details of VEM setup, and details on fitting of NR measurement (PDF)

The two-dimensional gap distribution and changes in the gap profile during sliding for PMA-C8 (EH) (applied load: 12.75 mN; sliding speed: 0.06 mm/s (1 Hz)) (mp4)

AUTHOR INFORMATION

Corresponding Author

*Kenji Fukuzawa; Email: fukuzawa@nuem.nagoya-u.ac.jp

*Yuxi Song; Email: yuxi_song@outlook.com

Notes

The authors declare no competing financial interest.

ACKNOWLEDGMENT

This study was partially supported by KAKENHI (20H00214), ENEOS Corporation, and JST SPRING, Grant Number JPMJSP2125. The neutron experiment at the Materials and Life Science Experimental Facility of the J-PARC was performed under a user program (2022A0072). The authors would like to thank Dr. Weiqi Shen for his support of measurements with the neutron reflectometry. Yuxi Song would like to take this opportunity to thank the “Interdisciplinary

Frontier Next-Generation Researcher Program of the Tokai Higher Education and Research System."

REFERENCES

(1) Habibi, Y.; Lucia, L. A.; Rojas, O. J. Cellulose Nanocrystals: Chemistry, Self-Assembly, and Applications. Chem. Rev. **2010**, 110 (6), 3479–3500. https://doi.org/10.1021/cr900339w.

(2) Liu, X.; Ma, P. X. Polymeric Scaffolds for Bone Tissue Engineering. Annals of Biomedical Engineering **2004**, 32 (3), 477–486. https://doi.org/10.1023/B:ABME.0000017544.36001.8e.

(3) Zelikin, A. N. Drug Releasing Polymer Thin Films: New Era of Surface-Mediated Drug Delivery. ACS Nano **2010**, 4 (5), 2494–2509. https://doi.org/10.1021/nn100634r.

(4) Smeeth, M.; Spikes, H.; Gunsel, S. Boundary Film Formation by Viscosity Index Improvers. Tribology Transactions **1996**, 39 (3), 726–734. https://doi.org/10.1080/10402009608983590.

(5) Spikes, H. Friction Modifier Additives. Tribol Lett **2015**, 60 (1), 5. https://doi.org/10.1007/s11249-015-0589-z.

(6) Müller, M.; Topolovec-Miklozic, K.; Dardin, A.; Spikes, H. A. The Design of Boundary Film-Forming PMA Viscosity Modifiers. Tribology Transactions **2006**, 49 (2), 225–232. https://doi.org/10.1080/05698190600614833.

(7) Fan, J.; Müller, M.; Stöhr, T.; Spikes, H. A. Reduction of Friction by Functionalised Viscosity Index Improvers. Tribol Lett **2007**, 28 (3), 287–298. https://doi.org/10.1007/s11249-007-9272-3.

(8) Gmür, T. A.; Mandal, J.; Cayer-Barrioz, J.; Spencer, N. D. Towards a Polymer-Brush-Based Friction Modifier for Oil. Tribology Letters **2021**, 69 (4), 124. https://doi.org/10.1007/s11249-021-01496-w.

(9) Tohyama, M.; Ohmori, T.; Murase, A.; Masuko, M. Friction Reducing Effect of Multiply Adsorptive Organic Polymer. Tribology International **2009**, 42 (6), 926–933. https://doi.org/10.1016/j.triboint.2008.12.012.

(10) Muraki, M.; Nakamura, K. Film-Forming Properties and Traction of Non- Functionalized Polyalkylmethacrylate Solutions under Transition from Elastohydrodynamic Lubrication to Thin-Film Lubrication. Proceedings of the Institution of Mechanical Engineers, Part J: Journal of Engineering Tribology **2010**, 224 (1), 55–63. https://doi.org/10.1243/13506501JET644.

(11) Cosimbescu, L.; Robinson, J. W.; Zhou, Y.; Qu, J. Dual Functional Star Polymers for Lubricants. RSC Adv. **2016**, 6 (89), 86259–86268. https://doi.org/10.1039/C6RA17461B.

(12) Schneider, H. M.; Frantz, P.; Granick, S. The Bimodal Energy Landscape When Polymers Adsorb. Langmuir **1996**, 12 (4), 994–996. https://doi.org/10.1021/la950556d.

(13) O'Shaughnessy, B.; Vavylonis, D. Non-Equilibrium in Adsorbed Polymer Layers. J. Phys.: Condens. Matter **2005**, 17 (2), R63–R99. https://doi.org/10.1088/0953-8984/17/2/R01.

(14) O'Shaughnessy, B.; Vavylonis, D. Irreversibility and Polymer Adsorption. Phys. Rev. Lett. **2003**, 90 (5), 056103. https://doi.org/10.1103/PhysRevLett.90.056103.

(15) O'Shaughnessy, B.; Vavylonis, D. Irreversible Adsorption from Dilute Polymer Solutions. Eur. Phys. J. E **2003**, 11 (3), 213–230. https://doi.org/10.1140/epje/i2003-10015-9.

(16) Zuo, B.; Zhou, H.; Davis, M. J. B.; Wang, X.; Priestley, R. D. Effect of Local Chain Conformation in Adsorbed Nanolayers on Confined Polymer Molecular Mobility. Phys. Rev. Lett. **2019**, 122 (21), 217801. https://doi.org/10.1103/PhysRevLett.122.217801.

(17) Gin, P.; Jiang, N.; Liang, C.; Taniguchi, T.; Akgun, B.; Satija, S. K.; Endoh, M. K.; Koga, T. Revealed Architectures of Adsorbed Polymer Chains at Solid-Polymer Melt Interfaces. Phys. Rev. Lett. **2012**, 109 (26), 265501. https://doi.org/10.1103/PhysRevLett.109.265501.

(18) Jiang, N.; Shang, J.; Di, X.; Endoh, M. K.; Koga, T. Formation Mechanism of High-Density, Flattened Polymer Nanolayers Adsorbed on Planar Solids. Macromolecules **2014**, 47 (8), 2682–2689. https://doi.org/10.1021/ma5003485.

(19) Sen, M.; Jiang, N.; Cheung, J.; Endoh, M. K.; Koga, T.; Kawaguchi, D.; Tanaka, K. Flattening Process of Polymer Chains Irreversibly Adsorbed on a Solid. ACS Macro Lett. **2016**, 5 (4), 504–508. https://doi.org/10.1021/acsmacrolett.6b00169.

(20) Napolitano, S. Irreversible Adsorption of Polymer Melts and Nanoconfinement Effects. Soft Matter **2020**, 16 (23), 5348–5365. https://doi.org/10.1039/D0SM00361A.

(21) Yamashita, N.; Hirayama, T.; Yamada, N. L.; Watanabe, H.; Onodera, K.; Sato, T. Highly Swollen Adsorption Layer Formed by Polymeric Friction Modifier Providing Low

Friction at Higher Temperature. Tribol Lett **2021**, 69 (2), 65. https://doi.org/10.1007/s11249-021-01443-9.

(22) Housmans, C.; Sferrazza, M.; Napolitano, S. Kinetics of Irreversible Chain Adsorption. Macromolecules **2014**, 47 (10), 3390–3393. https://doi.org/10.1021/ma500506r.

(23) Simavilla, D. N.; Huang, W.; Vandestrick, P.; Ryckaert, J.-P.; Sferrazza, M.; Napolitano, S. Mechanisms of Polymer Adsorption onto Solid Substrates. ACS Macro Lett. **2017**, 6 (9), 975–979. https://doi.org/10.1021/acsmacrolett.7b00473.

(24) Napolitano, S.; Wübbenhorst, M. The Lifetime of the Deviations from Bulk Behaviour in Polymers Confined at the Nanoscale. Nat Commun **2011**, 2 (1), 260. https://doi.org/10.1038/ncomms1259.

(25) Song, Y.; Fukuzawa, K.; Itoh, S.; Zhang, H.; Azuma, N. In-Situ Measurement of Temporal Changes in Thickness of Polymer Adsorbed Films from Lubricant Oil by Vertical-Objective-Based Ellipsometric Microscopy. Tribology International **2022**, 165, 107341. https://doi.org/10.1016/j.triboint.2021.107341.

(26) Fukuzawa, K.; Yoshida, T.; Itoh, S.; Zhang, H. Motion Picture Imaging of a Nanometer-Thick Liquid Film Dewetting by Ellipsometric Microscopy with a Submicrometer Lateral Resolution. Langmuir **2008**, 24 (20), 11645–11650. https://doi.org/10.1021/la802098w.

(27) K. Fukuzawa; Q. Liu; T. Tarukado; Y. Kajihara; R. Watanabe; S. Itoh; H. Zhang. Novel Methods for Real-Time Observation of Molecularly Thin Lubricant Films by Ellipsometric Microscopy: Application to Dewetting Observation. IEEE Transactions on Magnetics **2013**, 49 (6), 2530–2534. https://doi.org/10.1109/TMAG.2013.2247580.

(28) Fukuzawa, K.; Sasao, Y.; Namba, K.; Yamashita, C.; Itoh, S.; Zhang, H. Measurement of Nanometer-Thick Lubricating Films Using Ellipsometric Microscopy. Tribology International **2018**, 122, 8–14. https://doi.org/10.1016/j.triboint.2018.02.016.

(29) Namba, K.; Fukuzawa, K.; Itoh, S.; Zhang, H.; Azuma, N. Extension of Measurement Range of Lubrication Gap Shape Using Vertical-Objective-Type Ellipsometric Microscopy with Two Compensator Angles. Tribology International **2020**, 142, 105980. https://doi.org/10.1016/j.triboint.2019.105980.

(30) Yamada, N. L.; Torikai, N.; Mitamura, K.; Sagehashi, H.; Sato, S.; Seto, H.; Sugita, T.; Goko, S.; Furusaka, M.; Oda, T.; Hino, M.; Fujiwara, T.; Takahashi, H.; Takahara, A. Design and Performance of Horizontal-Type Neutron Reflectometer SOFIA at J-PARC/MLF. Eur. Phys. J. Plus **2011**, 126 (11), 108. https://doi.org/10.1140/epjp/i2011-11108-7.

(31) Hirayama, T.; Yamashita, N. Combined Use of Neutron Reflectometry and Frequency-Modulation Atomic Force Microscopy for Deeper Understanding of Tribology. Jpn. J. Appl. Phys. **2020**, 59 (SN), SN0803. https://doi.org/10.35848/1347-4065/ab9c43.

(32) Shen, W.; Hirayama, T.; Yamashita, N.; Adachi, M.; Oshio, T.; Tsuneoka, H.; Tagawa, K.; Yagishita, K.; Yamada, N. L. Relationship between Interfacial Adsorption of Additive Molecules and Reduction of Friction Coefficient in the Organic Friction Modifiers-ZDDP Combinations. Tribology International **2022**, 167, 107365. https://doi.org/10.1016/j.triboint.2021.107365.

(33) Hino, M.; Oda, T.; Kitaguchi, M.; Yamada, N. L.; Tasaki, S.; Kawabata, Y. The Ion Beam Sputtering Facility at KURRI: Coatings for Advanced Neutron Optical Devices. Nuclear

Instruments and Methods in Physics Research Section A: Accelerators, Spectrometers, Detectors and Associated Equipment **2015**, 797, 265–270. https://doi.org/10.1016/j.nima.2015.06.046.

(34) Glavic, A.; Björck, M. GenX 3: The Latest Generation of an Established Tool. J Appl Cryst **2022**, 55 (4), 1063–1071. https://doi.org/10.1107/S1600576722006653.

(35) Hansen, C. M. : : A User's Handbook, Second Edition, 2nd ed.; CRC Press: Boca Raton, 2007. https://doi.org/10.1201/9781420006834.

(36) Hansen, C. M. The three dimensional solubility parameter and solvent diffusion coefficient: Their importance in surface coating formulation; Danish Technical Press, 1967.

(37) Thees, M. F.; McGuire, J. A.; Roth, C. B. Review and Reproducibility of Forming Adsorbed Layers from Solvent Washing of Melt Annealed Films. Soft Matter **2020**, 16 (23), 5366–5387. https://doi.org/10.1039/D0SM00565G.

(38) Fleer, G.; Stuart, M. A. C.; Scheutjens, J. M. H. M.; Cosgrove, T.; Vincent, B. Polymers at Interfaces; Springer Science & Business Media, 1993.

(39) Zhu, H.; Dhopatkar, N.; Dhinojwala, A. Effect of Acid–Base Interactions on Conformation of Adsorbed Polymer Chains. ACS Macro Lett. **2016**, 5 (1), 45–49. https://doi.org/10.1021/acsmacrolett.5b00834.

(40) Linse, P. Effect of Solvent Quality on the Polymer Adsorption from Bulk Solution onto Planar Surfaces. Soft Matter **2012**, 8 (19), 5140. https://doi.org/10.1039/c2sm25074h.

(41) Lindvig, T.; Michelsen, M. L.; Kontogeorgis, G. M. A Flory–Huggins Model Based on the Hansen Solubility Parameters. Fluid Phase Equilibria **2002**, 203 (1), 247–260. https://doi.org/10.1016/S0378-3812(02)00184-X.

(42) Yamada, S.; Fujihara, A.; Yusa, S.; Tanabe, T.; Kurihara, K. Confined Film Structure and Friction Properties of Triblock Copolymer Additives in Oil-Based Lubrication. Polym J **2019**, 51 (1), 41–49. https://doi.org/10.1038/s41428-018-0114-y.

(43) Jiang, N.; Wang, J.; Di, X.; Cheung, J.; Zeng, W.; Endoh, M. K.; Koga, T.; Satija, S. K. Nanoscale Adsorbed Structures as a Robust Approach for Tailoring Polymer Film Stability. Soft Matter **2016**, 12 (6), 1801–1809. https://doi.org/10.1039/C5SM02435H.

(44) Jiang, N.; Sen, M.; Zeng, W.; Chen, Z.; Cheung, J. M.; Morimitsu, Y.; Endoh, M. K.; Koga, T.; Fukuto, M.; Yuan, G.; Satija, S. K.; Carrillo, J.-M. Y.; Sumpter, B. G. Structure-Induced Switching of Interpolymer Adhesion at a Solid–Polymer Melt Interface. Soft Matter **2018**, 14 (7), 1108–1119. https://doi.org/10.1039/C7SM02279D.

(45) Inutsuka, M.; Watanabe, H.; Aoyagi, M.; Yamada, N. L.; Tanaka, C.; Ikehara, T.; Kawaguchi, D.; Yamamoto, S.; Tanaka, K. Effect of Oligomer Segregation on the Aggregation State and Strength at the Polystyrene/Substrate Interface. ACS Macro Lett. **2022**, 11 (4), 504–509. https://doi.org/10.1021/acsmacrolett.2c00062.

(46) Inutsuka, M.; Haraguchi, M.; Ozawa, M.; Yamada, N. L.; Tanaka, K. Adhesion Control of Elastomer Sheet on the Basis of Interfacial Segregation of Hyperbranched Polymer. ACS Macro Lett. **2019**, 8 (3), 267–271. https://doi.org/10.1021/acsmacrolett.8b00971.

(47) Jahn, S.; Klein, J. Hydration Lubrication: The Macromolecular Domain. Macromolecules **2015**, 48 (15), 5059–5075. https://doi.org/10.1021/acs.macromol.5b00327.